Defense Threat Reduction Agency
8725 John J. Kingman Road, MS
6201 Fort Belvoir, VA 22060-6201

DTRA-TR-16-32

TECHNICAL REPORT

Investigation of Micro-Scale Laser-Powered Dielectric Particle-Accelerators with Potential Application in the Long Range Sensing of Fissile Material Grant

July 2018

HDTRA1-09-1-0043

Gil Travish

Prepared by:
UCLA Department of Physics & Astronomy
475 Portola Plaza
Los Angeles, CA 90095

DESTRUCTION NOTICE:

Destroy this report when it is no longer needed.
Do not return to sender.

PLEASE NOTIFY THE DEFENSE THREAT REDUCTION AGENCY, ATTN: DTRIAC/ RD-NTF, 8725 JOHN J. KINGMAN ROAD, MS-6201, FT BELVOIR, VA 22060-6201, IF YOUR ADDRESS IS INCORRECT, IF YOU WISH IT DELETED FROM THE DISTRIBUTION LIST, OR IF THE ADDRESSEE IS NO LONGER EMPLOYED BY YOUR ORGANIZATION.

REPORT DOCUMENTATION PAGE

Form Approved
OMB No. 0704-0188

1. REPORT DATE *(DD-MM-YYYY)*	**2. REPORT TYPE**	**3. DATES COVERED** *(From - To)*
00-07-2018	Technical	April 16, 2009 - July 20, 2015

4. TITLE AND SUBTITLE

Investigation of Micro-Scale Laser-Powered Dielectric Particle-Accelerators with Potential Application in the Long Range Sensing of Fissile Material

5a. CONTRACT NUMBER

5b. GRANT NUMBER
HDTRA1-09-1-0043

5c. PROGRAM ELEMENT NUMBER

6. AUTHOR(S)
Gil Travish

5d. PROJECT NUMBER

5e. TASK NUMBER

5f. WORK UNIT NUMBER

7. PERFORMING ORGANIZATION NAME(S) AND ADDRESS(ES)
UCLA Department of Physics & Astronomy
475 Portola Plaza
Los Angeles, CA 90095

8. PERFORMING ORGANIZATION REPORT NUMBER

9. SPONSORING / MONITORING AGENCY NAME(S) AND ADDRESS(ES)
Defense Threat Reduction Agency
8725 John J. Kingman Road, STOP 6201
Fort Belvoir, VA 22060-6201

10. SPONSOR/MONITOR'S ACRONYM(S)
DTRA

11. SPONSOR/MONITOR'S REPORT NUMBER(S)
DTRA-TR-16-32

12. DISTRIBUTION / AVAILABILITY STATEMENT
Distribution Statement A. Approved for public release; distribution is unlimited.

13. SUPPLEMENTARY NOTES

14. ABSTRACT

Advanced accelerators have been proposed to increase by orders of magnitude over conventional approaches the energy gained per unit distance, or gradient, in charged particle beams. The higher the gradient an accelerating structure can support and be powered to, the shorter length of device needed to reach a particular energy. These advanced accelerator schemes therefore promise to reduce the size (and cost) of major scientific instruments and medical and industrial systems. Dielectric Laser Accelerators (DLAs) are a class of advanced accelerators that use optical-scale structures powered by lasers to achieve these high gradients. We report on the first demonstration of acceleration within a resonant DLA. The structure required complex modeling and fabrication methods to realize the results the results here serve as a proof of principle and confirmation of the physics and technical ability underlying this approach to acceleration, and open the possibility of bread-box sized light sources.

15. SUBJECT TERMS
laser, particle accelerators, particle beams, dielectric

16. SECURITY CLASSIFICATION OF:			**17. LIMITATION OF ABSTRACT**	**18. NUMBER OF PAGES**	**19a. NAME OF RESPONSIBLE PERSON**
a. REPORT	**b. ABSTRACT**	**c. THIS PAGE**	SAR	27	Dave Petersen
Unclassified	Unclassified	Unclassified			**19b. TELEPHONE NUMBER** *(include area code)* 571-616-3164

UNIT CONVERSION TABLE

U.S. customary units to and from international units of measurement*

U.S. Customary Units	Multiply by → / ← Divide by†		International Units
Length/Area/Volume			
inch (in)	2.54	$\times 10^{-2}$	meter (m)
foot (ft)	3.048	$\times 10^{-1}$	meter (m)
yard (yd)	9.144	$\times 10^{-1}$	meter (m)
mile (mi, international)	1.609 344	$\times 10^{3}$	meter (m)
mile (nmi, nautical, U.S.)	1.852	$\times 10^{3}$	meter (m)
barn (b)	1	$\times 10^{-28}$	square meter (m^2)
gallon (gal, U.S. liquid)	3.785 412	$\times 10^{-3}$	cubic meter (m^3)
cubic foot (ft^3)	2.831 685	$\times 10^{-2}$	cubic meter (m^3)
Mass/Density			
pound (lb)	4.535 924	$\times 10^{-1}$	kilogram (kg)
unified atomic mass unit (amu)	1.660 539	$\times 10^{-27}$	kilogram (kg)
pound-mass per cubic foot (lb ft^{-3})	1.601 846	$\times 10^{1}$	kilogram per cubic meter (kg m^{-3})
pound-force (lbf avoirdupois)	4.448 222		newton (N)
Energy/Work/Power			
electron volt (eV)	1.602 177	$\times 10^{-19}$	joule (J)
erg	1	$\times 10^{-7}$	joule (J)
kiloton (kt) (TNT equivalent)	4.184	$\times 10^{12}$	joule (J)
British thermal unit (Btu) (thermochemical)	1.054 350	$\times 10^{3}$	joule (J)
foot-pound-force (ft lbf)	1.355 818		joule (J)
calorie (cal) (thermochemical)	4.184		joule (J)
Pressure			
atmosphere (atm)	1.013 250	$\times 10^{5}$	pascal (Pa)
pound force per square inch (psi)	6.984 757	$\times 10^{3}$	pascal (Pa)
Temperature			
degree Fahrenheit (^oF)	$[T(^oF) - 32]/1.8$		degree Celsius (^oC)
degree Fahrenheit (^oF)	$[T(^oF) + 459.67]/1.8$		kelvin (K)
Radiation			
curie (Ci) [activity of radionuclides]	3.7	$\times 10^{10}$	per second (s^{-1}) [becquerel (Bq)]
roentgen (R) [air exposure]	2.579 760	$\times 10^{-4}$	coulomb per kilogram (C kg^{-1})
rad [absorbed dose]	1	$\times 10^{-2}$	joule per kilogram (J kg^{-1}) [gray (Gy)]
rem [equivalent and effective dose]	1	$\times 10^{-2}$	joule per kilogram (J kg^{-1}) [sievert (Sv)]

*Specific details regarding the implementation of SI units may be viewed at http://www.bipm.org/en/si/.

†Multiply the U.S. customary unit by the factor to get the international unit. Divide the international unit by the factor to get the U.S. customary unit.

Introduction & Background

Particle accelerators, which reached maturity as research tools decades ago, have had deep impact in discovery science and have become essential tools for broader society. In recent years, continued advances in accelerator physics and technology have enabled fundamental physics discoveries by extending the energy frontier to unprecedented heights. However, these modern facilities depend on technology, based on microwave-driven resonant cavities, that is largely unchanged since the 1940s. The typical rate of energy gain per meter (the "energy gradient") has not grown significantly, and consequently higher collider energies require larger and larger facilities. While refinements in cavity design and materials (especially the use of superconductors) have gradually improved the energy gradients attainable in modern structures to more than 100 MeV/m, fundamental physics and engineering limitations are likely to prevent this number from increasing significantly in the future. At the same time, it is clear that simply continuing to build larger and larger accelerators is, or soon will be, practically and financially impossible. Future increases in collider energies must rely on new methods of acceleration that can deliver far higher gradients. In addition, high-gradient acceleration mechanisms could enable industrial and medical accelerators to become far more compact and inexpensive.

In response to this need, the last two decades have seen intensive study of so-called advanced accelerator concepts, including designs based on beam-to-beam energy exchange, externally powered structures, and laser illumination of a solid or plasma. Some success has been achieved via the use of laser-plasma and laser-solid interactions to generate large accelerating fields, but these approaches have disadvantages relative to structure-based accelerators, including device complexity and lack of field control. This paper describes an advanced accelerator based on a laser-powered structure. Since energy gradient in a structure scales inversely with wavelength, moving from microwave- to laser-powered structures can increase the gradient by several orders of magnitude. These optical-scale field-shaping structures are collectively known as Dielectric Laser Accelerators (DLAs), and offer sustained accelerating fields in the GV/m range when powered by conventional short-pulse lasers with GW peak powers and mJ pulse energies illuminating millimeter areas. They offer a path toward compact, extreme high-gradient acceleration for high-energy physics applications as well as industrial and medical uses. Several DLA designs have been investigated by multiple groups in the last 10 years; they can be configured in a wide variety of geometries and support various accelerating modes. The use of dielectric, rather than metal, has two advantages: it offers increased resistance to electric breakdown, thereby increasing the maximum sustainable field within the structure; and it leverages a well-developed semiconductor industry, allowing fabrication of structures from various dielectric and semiconductor materials at the wafer scale and their replication in large quantities.

Several DLA designs are variations on photonic band-gap (PBG) structures—in which a defect in a periodic system acts to confine an accelerating mode—in one or two dimensions. The PBG fiber accelerator consists of a hollow-core fiber optic cable, in which the central defect supports an accelerating mode, and is under development at SLAC [13]; the "woodpile structure"[14] is a 3D PBG constructed from a silicon lattice that fully confines the accelerating fields, and was also developed at SLAC. These are both traveling-wave devices; without the benefits of resonant field enhancement, coupling laser into the structure successfully is challenging. The woodpile structure has also proven difficult to fabricate. A contrasting technology, the grating accelerator, has been developed and tested at Stanford; in that case, acceleration occurs via the near fields created by

illuminating a diffraction grating with a laser [15, 16]. This nonresonant structure may have wakefield limitations but is relatively simple to tune in energy. This device has been extensively studied and shown clear acceleration at high gradients. [17]

This project investigated a distinct DLA approach: a standing-wave structure with a resonant "cavity" formed between two reflectors. Power is side coupled along a periodic diffractive optic ("phase mask"). This structure is known as the Micro Accelerator Platform (MAP).

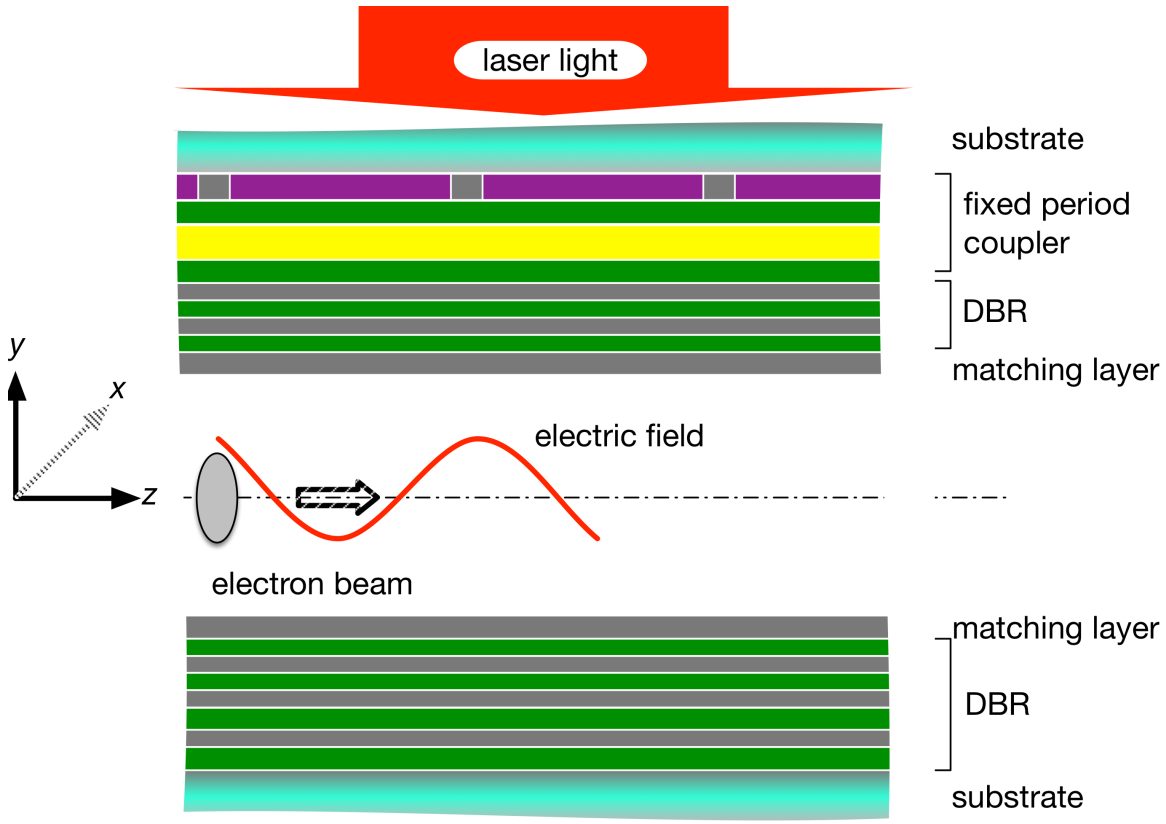

Figure 1: Cross-section of three periods of the Micro Accelerator Platform: the accelerating gap is shown in the middle, with the electron beam traversing from left to right; the drive laser is incident from the top and traverses a substrate (aqua), a diffractive optic coupler (purple, green, yellow, green) and finally a DBR (green/grey).

The MAP is built around a pair of all-dielectric Bragg reflectors, giving high breakdown resistance and scalability to various wavelengths (Figure 1). It is a low-Q structure that is well matched to existing laser technology (Table 1).

The structure was the subject of extensive simulation modeling including realistic materials and optical properties [12]. An optimal coupling scheme for laser power, involving a distributed grating element on the upper surface of the device, and the effects of coupling parameters on the accelerating mode have been extensively documented. Finally, prototype structures were built and tested experimentally, with transmission and acceleration observed, and modeled via 3D self-consistent simulation.

Table 1: Accelerator and power source parameters for the reference MAP DLA design. The enhancement factor here is 5.

Laser wavelength & Cell Length	800 nm
Effective gradient	0.5 GeV/m
Quality factor Q	800
Fill time	3 ps
Laser intensity	100 MW
Laser pulse length	3 ps
Energy gain per unit cell	~0.5 keV
Incident to Accelerating Field Ratio	1:5
Accelerating Field to Peak Structure Field	1:2

Experimental Methods

The technological motivation behind the structure design of many Dielectric Laser Accelerators (DLAs) is threefold:

1. Select an spectral range where materials with good properties exist;
2. Select an operating wavelength where high-power sources commonly exist;
3. Design a structure geometry that supports the desired electromagnetic mode for particle acceleration and can be fabricated with established methods.

These considerations typically drive DLA design towards optical and near-IR wavelengths. Other considerations determine how the accelerating mode will be produced and supported within the structure. In PBG-based devices, the mode is confined with a minimal interaction with the material ("walls") of the structure; however, coupling of the mode into the PBG is often challenging. These devices are often non-resonant, and as such require that the peak incident field be the same as the peak accelerating field. In the MAP structure described here, a resonant accelerating mode is established in the gap between two slab-symmetric reflectors. This mode's peak field can have an "enhancement factor" of several times the incident field. The input coupler is a simple diffractive optic similar to a transmissive grating or phase mask. Because of the open geometry near the accelerating axis, there is no mode confinement beyond that established by the incident field. This configuration allows for large-aspect-ratio flat beams to be used as a method to increase the allowed charge and reduce the space charge forces. In simulations it has been shown that while there is no structural mode-confinement, the limited diffraction in the gap, incident field distribution and enhancement factor contribute to a transversely-localized mode.

The longitudinal electric field of the MAP's standing wave resonant mode is responsible for the acceleration of electrons traversing it. In order to achieve synchronous acceleration, its periodicity matches the distance travelled by an electron with velocity βc during one optical cycle of the incident laser ($1/2\pi\omega$). The longitudinal wave vector and field thus take the form:

$$k_z = \frac{\omega}{\beta c}$$

$$E_z = E_0 \cos k_z z \ \cosh\left(\frac{k_z y}{\gamma_s}\right)\cos(\omega t + \varphi_0)$$

This resonance of the MAP has been characterized with extensive simulation work detailing its field enhancement, quality factor, fill time, and transverse field variation and is described in our prior publications (see list in the Appendix). An example of the simulated resonant fields is given in Figure 2, and the structure dimensions are shown in Figure 3.

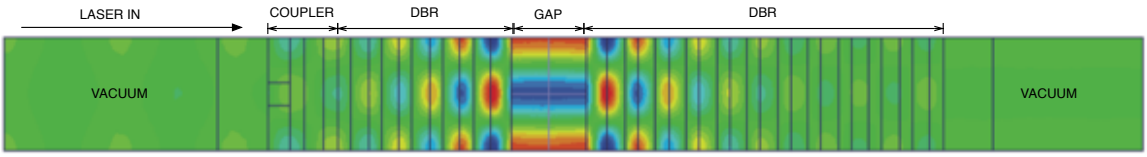

Figure 2: MAP accelerating fields of a single-period of the MAP structure, simulated in HFSS (false color represents magnitude of electric field in the beam propagation direction. The laser impinges from the left. The electron beam travels from bottom to top through the gap. The gap in the middle shows slightly scalloped fields, as one would expect from a realistic structure.

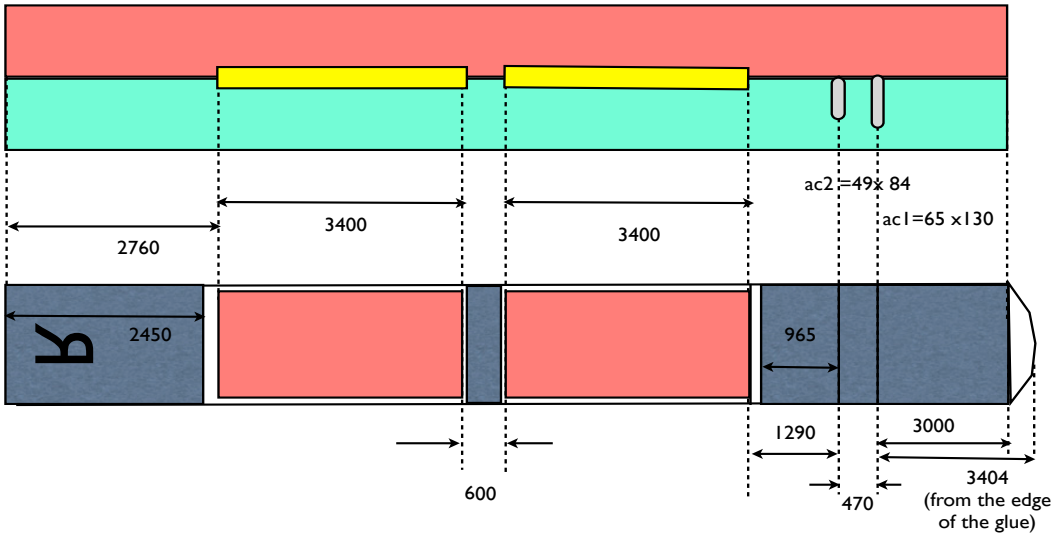

Figure 3: Dimensions of MAP structure and acceleration channels (colored in yellow), ac1 and ac2 refer to alignment channels 1 and 2.

Equipment

The MAP structures as built measured 1.0 ± 0.1 mm in length and 1.00 ± 0.01 mm in thickness, with a transverse area of 3.3 mm, comprising 1250 optical periods. A combination of methods from the photonics and microelectronics industries, including lithography, lift-off, etching, polishing and thin-film deposition, were used to fabricate the top and bottom halves of the structures on fused silica substrates. In practice, dozens to hundreds of half-structures were fabricated at once on 100 mm (diameter) wafers (Figure 4). The two halves of the structure were fabricated separately, on different wafers; following measurement of the thin-film thicknesses, the two wafers were bonded, using spacers to fix the vacuum gap size at 400 nm (one-half optical wavelength). (Required tolerances on the gap spacing are set by the need to preserve the quality of the accelerating mode, and are estimated via simulation to be ±15%.) Finally, individual structures were separated by dicing, and each structure was checked for quality both visually and optically. Figure 5 is an optical micrograph of a completed MAP structure.

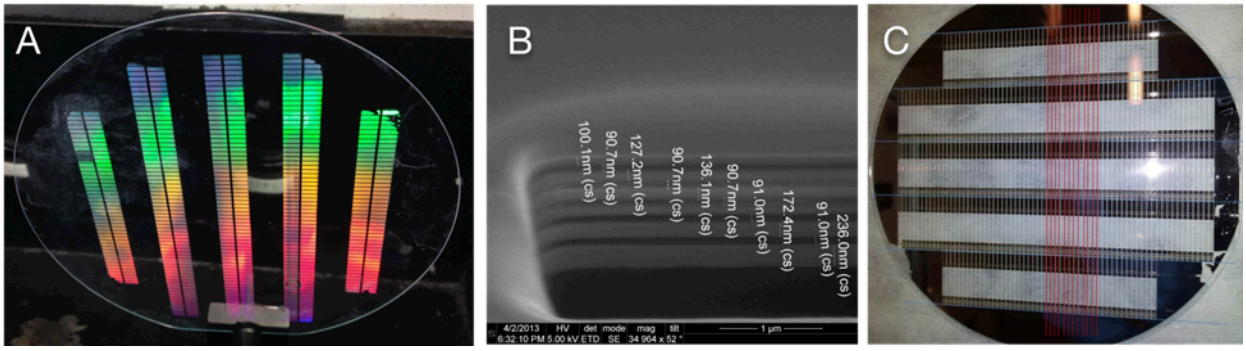

Figure 4: Fabrication: (A) White light reflection from thin films of structures (about 400 each) on silicon dioxide wafer; (B) SEM image of top Bragg layers for one structure, in cross section; (C) Top full-wafer view of an array of MAP structures prior to dicing; green and red lines are dicing guides.

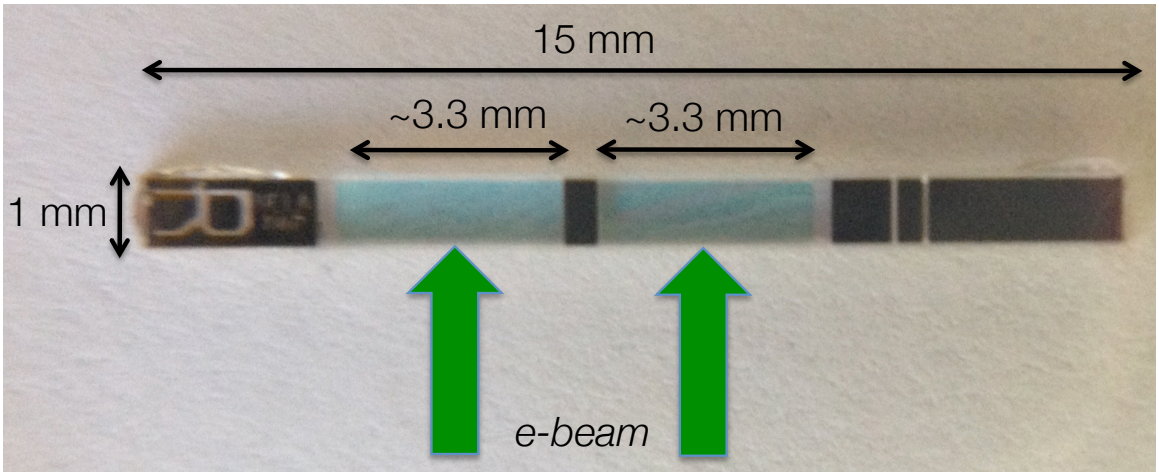

Figure 5: Photograph (top view) of two completed MAP structures, side by side on a single substrate. The active areas (acceleration channels) appear pale blue. The electron beam path is indicated by green arrows. The two narrow stripes visible on the right side of the structure are 50×100 μm channels for beam alignment during the experiment.

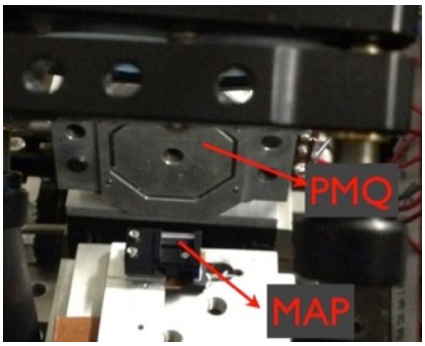

Figure 6: MAP installed at E163 beam line.

Further details of the fabrication and characterization processes have been given in the literature (see references at the end of the Appendix). Several approaches for bonding have been explored, with varying challenges and levels of success. We also note that establishing and determining the exact gap height has been and continues to be a significant technological challenge. Spectrophotometer

measurements of the Bragg layers have been successful in establishing thin-film thicknesses in larger portions of the wafers [Travish et al., IPAC 2012; Sozer et al., PPPS 2013], but lack sufficient resolution to detect the resonant accelerating mode in the 400-nm gap. Alternative approaches to fabricating the structure would likely eliminate these problems (as a ~100 nm feature is well within state-of-the-art for lithography), but would require additional development.

Table 2: Structure parameters as measured along with error or uncertainty (where known).

Parameter	**Measured Value**
Period	800 nm
Gap	(400 ± 20) nm
Length	(1.0 ± 0.1) mm
Number of periods	1250
Total Thickness	1 mm ± 10 μm

Setup

Acceleration tests of the MAP structures were carried out using the E-163 beamline at the SLAC National Accelerator Laboratory's NLCTA facility (Figure 6). The E-163 beamline, with an energy of 60 MeV, is well instrumented for installing and measuring laser-driven accelerators, including a multi-axis precision positioning stage for structure mounting, camera-based alignment methods, and a high-resolution energy spectrometer. An rf photocathode gun produces electron bunches at a 10 Hz repetition rate, which are pre- accelerated to 60 MeV in an X-band linac before interacting with the DLA. The energy spread of each electron bunch is 10 keV, but the shot-to-shot jitter can approach 70 keV when system conditions are poor. To reduce the energy jitter and spread, collimating jaws are employed in the middle of a chicane after the linac. After passing through the chicane, the beam is sent through a "dogleg" transport line and into the experimental hall. (This dogleg, a strongly dispersive element, can cause positional jitter and orbit deviation at the IP.) In the experimental hall, the beam passes through 6 final focusing quads and then through a triplet of permanent magnetic quadrupoles. A diagram of the final section of the beamline is given in Figure 6 are summarized in Table 3.

For acceleration tests, the MAP structure is installed on a positioning stage at the final beam focus, and its upper surface is illuminated by an 800-nm Ti:Sapphire laser, with the laser pulse length matched to the fill time of the MAP accelerator (5 ps). The laser spot is highly asymmetric in order to match the dimensions of the acceleration channel.

Table 3: Typical electron beam and laser parameters during MAP tests at NLCTA.

Parameter	**Value**
Beam energy	60 MeV
Energy jitter (without collimation)	±50–70 keV
Energy spread (FWHM, without collimation)	10 keV
Charge per bunch (without collimation)	10 pC
Electron bunch length (FWHM)	1 ps
Beam spot size (FWHM) at IP	
Vertical	(25 ± 10) μm

Horizontal	(50 ± 25) μm
Beam emittance (normalized rms)	2-10 μm
Laser pulse length	5 ps
Laser spot size at MAP surface	
Transverse (x)	50 μm
Axial (z)	1 mm

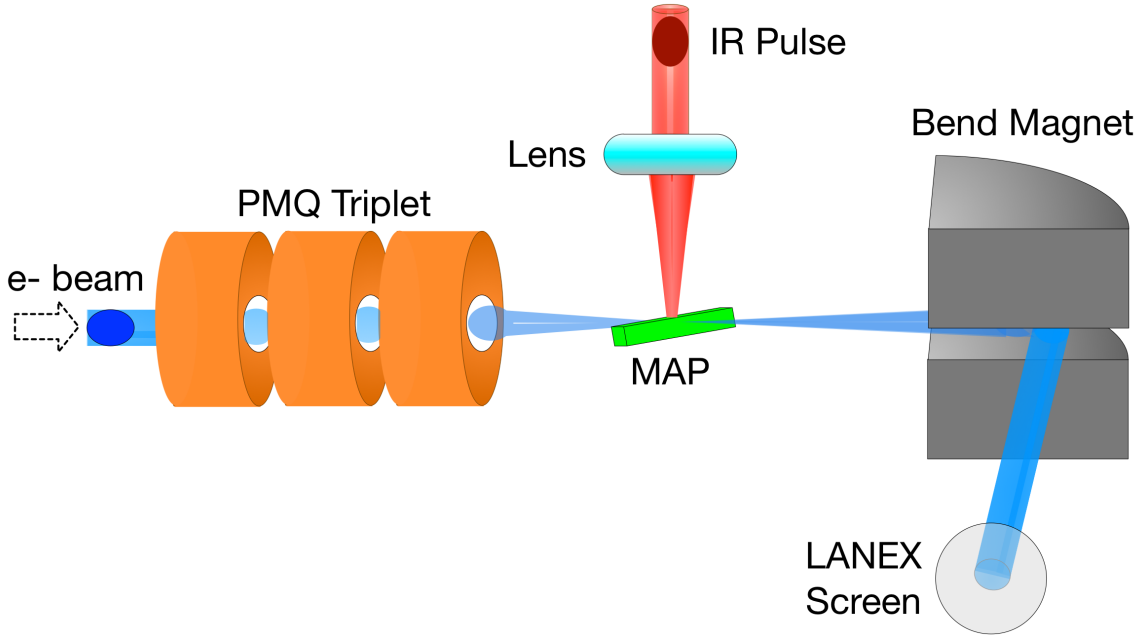

Figure 6: Sketch of the experimental arrangement: The electron beam is incident from the left; the laser from the top. Permanent magnet quadrupole magnets serve as a final focusing optic for the electron beam onto the structure (placed on a micropositioning platform, not shown). After the interaction, the electron beam is sent around a high-resolution bend spectrometer and imaged on a florescent screen using an intensified camera (not shown).

Procedures

Successful acceleration requires precise alignment of structure, electron beam, and laser along three axes, as well as temporal overlap of electron beam and laser. If the structure is misaligned by rotation in the horizontal plane (i.e., around the *x*-axis in Figure 1), the effective period seen by the beam is increased and the resonance condition will not be met. Likewise, if the structure is tilted forward or backward relative to the horizontal plane (that is, rotated around the *y*-axis in Figure 1), period-to-period phase variation is introduced and synchronous acceleration is prevented. To carry out initial alignment, the electron beam is imaged at the IP and spectrometer; alignment of beam to structure axis is initially done by eye and then optimized by maximizing beam transmission through one of the 30x100 μm alignment channels added to the MAP wafer, as the tip and tilt angles of the stage are varied. To control for perpendicular incidence of the laser on the upper surface of the structure, we bring the angle between the reflected laser signal and incident beam to zero, using a beam splitter in the laser path; this produces alignment to a precision of ±0.01°. Transverse spatial overlap of the laser and electron beams is confirmed by a camera focused on the rear of the MAP structure, which images both optical transition radiation (OTR) from the electron beam transiting the glass and reflections of the laser from the layers of the structure. As the two beam sizes are of

the same order, the laser spot centroid is varied by approximately half a spot width to ensure optical overlap with the electron trajectory.

Temporal overlap of the electron beam and laser is initially accomplished by propagating the electron OTR light (produced when it impacts the structure) to a fast photodiode located downstream from the electron spectrometer, where it is overlapped with the laser beam. This produces synchronization within the rise time of the photodiode, 50 ps. However, the resonant structure mode exists for a far smaller time (the structure fill time is only 5 ps), and the photodiode resolution is therefore insufficient to ensure interaction between electrons and laser fields. To achieve true temporal overlap, a voice coil in the laser path pseudo-randomly varies the laser path length over a length of 18 mm in a Halton sequence, producing ±50 ps variation in the laser timing. Over runs of hundreds of laser shots, all possible delays within this window are sampled, while the voice coil position is recorded; thus, it is possible to correlate output energy spectra with laser-electron delay time, and to establish the precise timing range over which acceleration is seen to occur.

The beam spot size, roughly 50 μm diameter, is far larger than the aperture of the MAP structure (400 nm vertically x 3 mm horizontally). The majority of the electrons will travel through the dielectric material rather than the vacuum gap; in so doing they will lose energy via scattering, at a rate on the order of several hundred keV/mm. Only those electrons transmitted through the vacuum gap will emerge with their injection energy. The measured energy spectrum in the absence of laser fields within the structure thus shows two peaks: the larger one, at lower energy, is the scattered beam, with a small peak at 60 MeV containing the transmitted beam.

Since only the transmitted population will experience the accelerating fields in the vacuum gap, the signature of acceleration is then a broadening of the transmitted spectral peak: as the electron bunch is typically two orders of magnitude longer than a structure period, electrons are injected into all possible phases of the accelerating field and experience both positive and negative energy modulation. Electrons near the optimal phase for acceleration or deceleration will tend to be trapped and bunched, enhancing the energy distribution at its high and low extremes, with the resulting shape having a "double-horned" appearance, as simulated in Figure 7.

Simulation Results

To model the performance of the MAP, a combination of simulation codes was necessary. The trajectory of the injected electron beam through the NLCTA beamline was modeled using `elegant`. Beams arriving at the MAP are then divided into separate populations: those that traverse the vacuum cavity, and those that pass through the MAP substrate itself. The scattering and energy loss of particles passing through the dielectric material are modeled using the `GEANT4`-based code `G4beamline` to generate a downstream energy profile. Acceleration within the vacuum gap is modeled self-consistently using `VORPAL`, which includes the buildup of resonance within the structure after laser illumination, followed by energy modulation of the injected beam in the resonant fields. The two populations are then recombined and tracked through the magnetic spectrometer to obtain the predicted acceleration signal. Figure 7 shows an example of the expected acceleration signal produced by this combination of models.

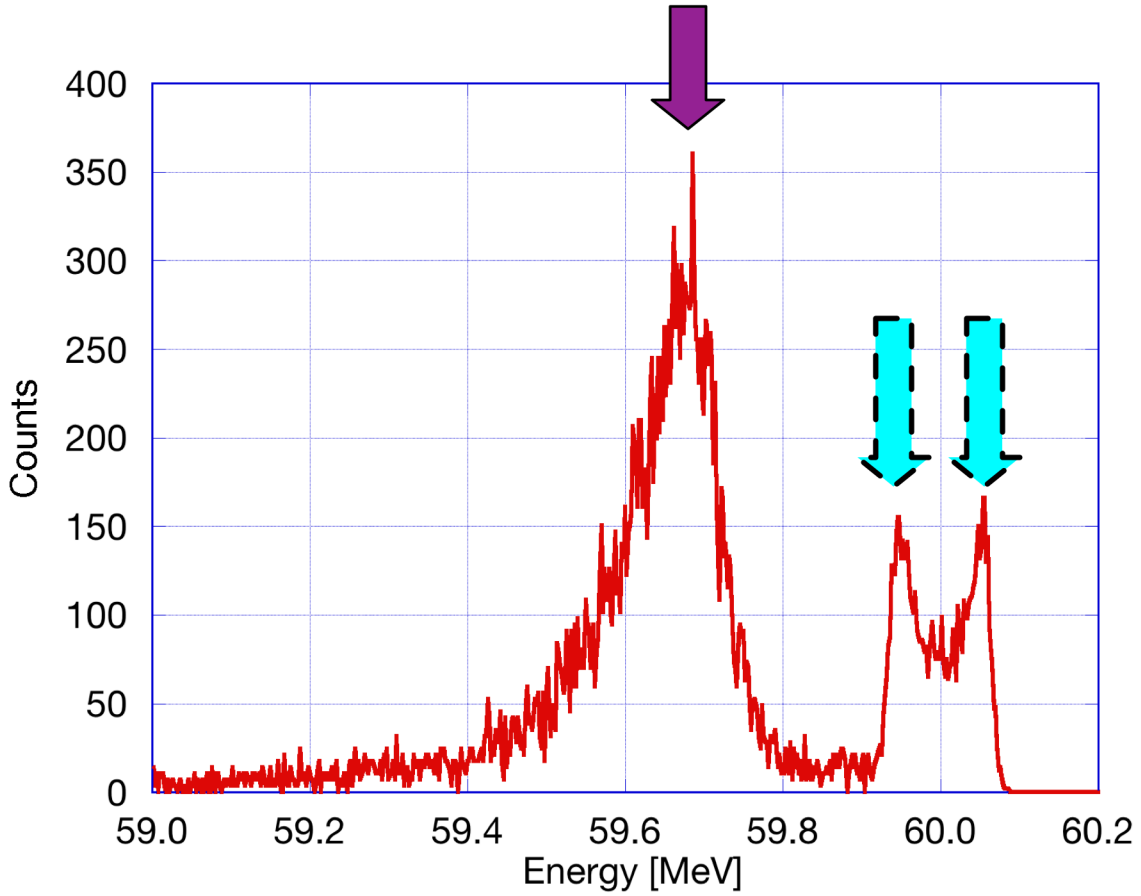

Figure 7: Simulated energy distribution of an electron bunch after having traveled through the MAP with a peak accelerating-field of 0.4 GV/m. The large peak on the left (purple arrow) consists of electrons that transited the MAP substrate and were scattered; the smaller "double-horned" distribution on the right (cyan arrows) shows positive and negative energy modulation of electrons transiting the vacuum gap.

The random sampling of electron-laser delay times, discussed above, means that searching for acceleration in the structure is a statistical process. For a given structure position, alignment, and beam tune, several hundred laser shots are collected at a repetition rate of 10 Hz. An automated data

acquisition system records spectrometer images for each shot and fits the resulting spectrum to a combination of analytic functions, with the goal of identifying shots showing the expected broadening of the energy spectrum of the transmitted beam. Shots for which the injected beam is not well tuned can also be eliminated, by applying similar fits to the spectrum of the scattered beam and measuring its energy centroid and spread, as discussed below. Other system variables (e.g., beam charge, laser energy and structure position) are also logged for later analysis.

The injected beam's energy jitter (±50–70 keV) was comparable to the expected energy modulation via acceleration. A series of software filters were used to reduce the statistical noise, as follows: (i) Gaussian fits were applied to the spectral peak due to unaccelerated (scattered) particles that traveled through the structure material, and the scattered peak's energy centroid and spread were determined. (ii) Shots in which the scattered peak width exceeded 300 keV (FWHM), indicating an increase in initial beam energy spread due to phase drift upstream of the experiment, were removed; (iii) Shots in which the scattered peak centroid was shifted by more than ~50 keV from its optimal range, indicating fluctuations in pointing, were removed; (iv) Periods of stable and unstable beam parameters were identified by measuring the shot-to-shot variability of the scattered peak width: periods with large standard deviation in the scattered peak widths were associated with unstable operation and were removed. After these three filtering steps, the variation in transmitted peak width (with laser off) was reduced to ±11 keV, which is 3 to 5 times less than the magnitude of the expected acceleration.

Experimental Results

A total of eight experimental runs using the E-163 facility were performed over an 18-month period, as detailed in Table 4. Of those, two showed the expected signature of acceleration; the remaining runs illustrate the many challenges encountered during this work, particularly involving fabrication. Multiple structures were prepared for each run, in case of damage, but the difficulty of monitoring a structure's integrity during mounting at the IP, and during the experiment itself, can (and often did) lead to undetected failures. In what follows, we consider the results from Runs 6 and 9, in which acceleration was found.

Table 4: Summary of significant run campaigns, month & year performed, and key result. *Run 9 utilized a new structure design, expected to produce a higher-quality accelerating mode.

Run	Date	Key Result
1	APR12	No transmission found; structure collapsed.
2	JUN12	Transmission found.
3	—	Run skipped.
4	AUG12	Structures damaged due to poor bonding.
5	OCT12	New bonding. Machine failure prevented data collection.
6	DEC12	Found evidence of acceleration; structure damaged due to laser.
7	APR13	Structures were dimensionally incorrect.
8	JUN13	Good transmission. No acceleration. Laser damage along polishing marks.
9*	NOV13	Acceleration found using improved structure design.

After Run 8, inspection of the MAP structure revealed laser damage of the thin films. The damage was along the polishing lines that were generated during fabrication of the coupling layer of the structure. This indicates local sensitivity variation of the laser damage threshold dependent on fabrication processes. An image of the observed damage can be seen in Figure 8. The diagonal variation of the contrast is due to variation of the film thickness after polishing. The damaged areas 1 and 2 on the left are high intensity laser damage above the bulk laser damage threshold; however, damaged areas 3 and 4 on the right are just below the bulk damage threshold and appear along the polishing marks. Figure 8 (b) shows an electron microscopy image of the same areas.

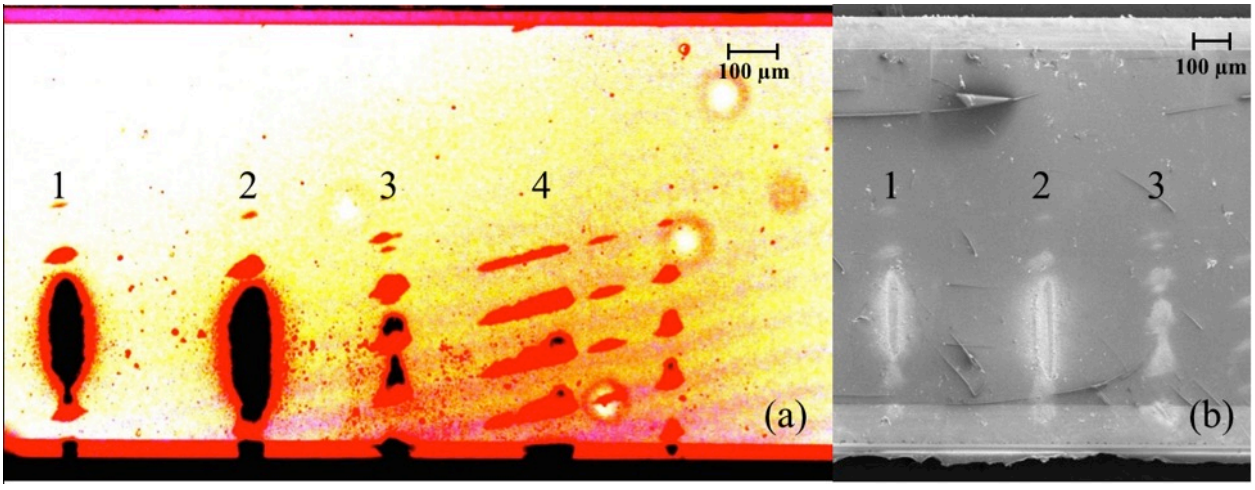

Figure 8: Laser damage of MAP structure used in Run 8 taken with (a) High-contrast optical microscopy (b) Scanning electron microscopy.

The unprocessed images of Figure 9, obtained during Run 6, and the processed energy spectra of Figure 11, obtained during Run 9, are typical energy spectra corresponding to successful acceleration. The large peak contains electrons that traveled through the structure material rather than the vacuum channel, losing roughly 300 keV due to scattering; this peak is insensitive to the presence of the laser field. The small peak on the right shows the expected signature of energy modulation: a "double-horned" distribution, with equal numbers of particles falling in accelerating and decelerating phases. The data is well fit by numerical simulation that models both the intra-dielectric scattering and the laser acceleration within the vacuum channel.

For the particular shot shown in the figure, a maximal energy gain of 56 keV (i.e., an acceleration gradient of 56 MV/m) was obtained with a laser fluence of 0.04 J/cm^2—20% of the predicted damage threshold—so is less than half of the possible peak acceleration gradient. This value for the fluence corresponds to a peak incident laser field of 31 MV/m, which—with a field enhancement factor $\eta \sim 4$ between the incoming laser fields and the standing-wave cavity mode—corresponds to a forward accelerating field of about 62 MV/m. The discrepancy between the predicted and measured values is likely due to several factors, including non-uniformity in the gap spacing, possible structure deformation during insertion, and variability in the local thin-film quality, each of which can modify the field enhancement factor significantly. We further speculate that occlusion of the gap and partial material damage due to the laser could hurt the field enhancement, alter the resonant frequency and affect the synchronicity of the electrons and the accelerating fields. These effects can also cause reduction in energy via a decreased interaction distance.

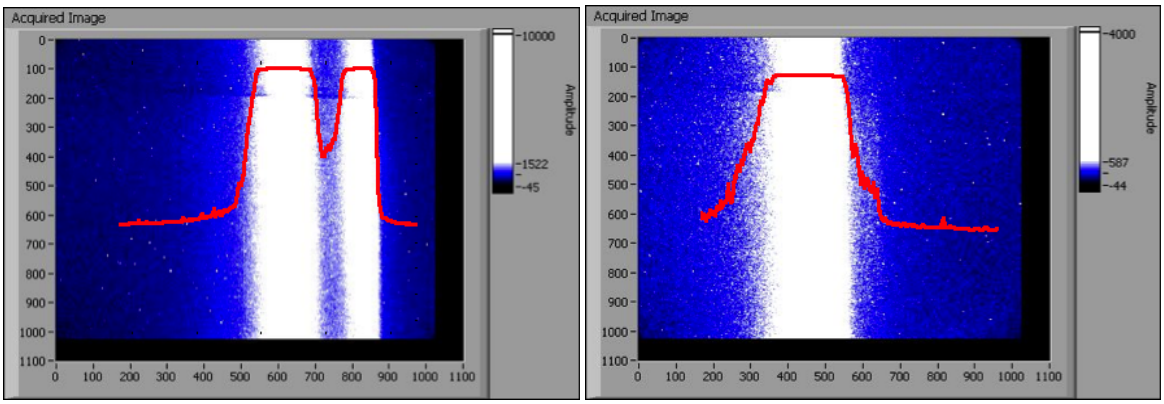

Figure 9. (Left) Transmission signal through an alignment channel. (Right) Weak transmission signal through an accelerating channel. In both cases the large signal on the left of the camera image (from the scintillating screen after the bend spectrometer) is the electron distribution scattered through the structure. The relatively small separation in energy between the scattered and transmitted populations in the right-hand image may be due to partial occlusion of the vacuum gap by peeling or buckling of adjacent dielectric layers.

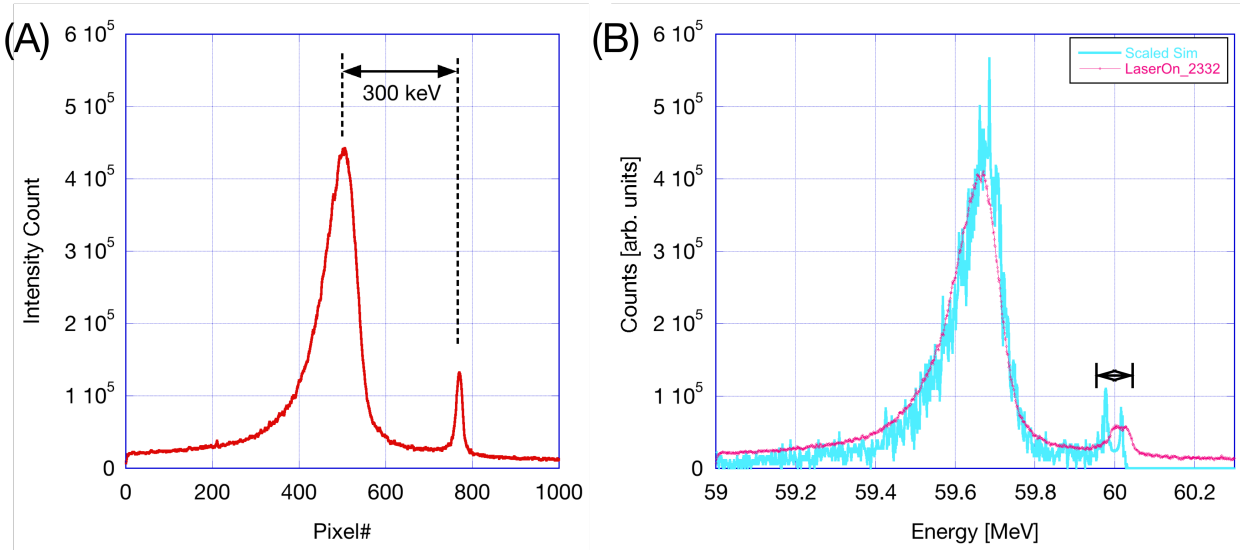

Figure 10: Sample raw experimental energy spectra after the IP, with no laser power (A) and with laser illumination creating an accelerating mode (B). The large peak contains electrons scattered by the structure; the small peak shows energy modulation of the transmitted beam, as described in the text. For each such spectrum, a calibration (approximately 1.3 keV/pixel) is used and a centroid is established (about pixel 790 for 60.0 MeV here). A comparison with scaled simulations is also shown in (B), and shows good agreement for identical laser parameters.

Figure 11 presents complete time-correlation data from the successful run. A clear signature of acceleration (in which the transmitted electron energy is modulated at the 3σ level compared to the baseline fluctuations) is visible for a laser-electron delay interval of 6–7 ps. The timing overlap is a highly sensitive parameter, requiring ±3 ps of accuracy for acceleration to be observed; this value is comparable to the structure fill time, as expected. As the enlargement in Figure 11 (b) makes clear, the dataset is both noisy and sparse in the region of interest; Figure 11 (c) shows a smoothed version of the data that more clearly indicates the region of acceleration, though the peak height is necessarily reduced. Fluctuations in the background are due primarily to variation in the energy and phase of the electron beam earlier in the beamline, which is visible as jitter in the pointing, energy, and energy spread of the beam incident on the MAP structure. This jitter is large enough that during many "laser-on" shots, the beam is in fact at the wrong energy or misaligned for successful acceleration. While filtering during data analysis was used to remove the most evident of these poor shots (as described in the Methods section), it is likely that some percentage of the remaining shots did not meet the conditions needed for successful injection. Further, since the acceleration signal was only discovered during post-analysis, we could not ensure that the time interval of interest was completely sampled. For these reasons, it is difficult to draw rigorous conclusions about the acceleration gradient demonstrated. However, a lower bound on the gradient can be inferred: with no laser, the mean width of the transmitted peak is 8.4 keV; with laser on, the maximally broadened peak reaches a width of 59 keV, implying an acceleration gradient of 28 MeV/m if the full 1 mm of structure is supporting fields. This data was obtained with a relatively low laser fluence of 0.027 J/cm^2, an order of magnitude below the predicted damage threshold of 0.2 J/cm^2. The simulation deviate from the experimental data in two notable ways: the overall energy spreads (vertical axis) are scaled (since the absolute acceleration in the simulated ideal structure results are greater), and the width of the simulated distribution is greater even when the pedestal of the minimum observable energy spread in the experiment (about 7 keV) is accounted for. Both of these discrepancies between the simulated and experimental results might be accounted for by the sub-optimal structure

performance. Unlike the good overlap agreement of Figure 10 which compares a single beam shot, the results of Figure 11 are taken over many (approximately 1000) beam shots where drifts and jitter can occur that are not modeled in the simulations.

This value for the fluence corresponds to a peak incident laser field of 31 MV/m, which—if we assume a field enhancement factor $\eta \sim 4$ between the incoming laser fields and the standing-wave cavity mode—corresponds to a forward accelerating field of about 62 MV/m. In addition to the sparse sampling, the difference between the predicted and measured values is likely also due to possible structure deformation during insertion, variation in thin-film quality, and degradation of the structure during the experiment. Post-inspection showed occlusion of the gap by peeling or buckling of adjacent dielectric layers, and partial laser damage to the structure. This would result both in a decreased interaction length, as some portion of the structure periods are no longer resonant, and in degradation of the field enhancement.

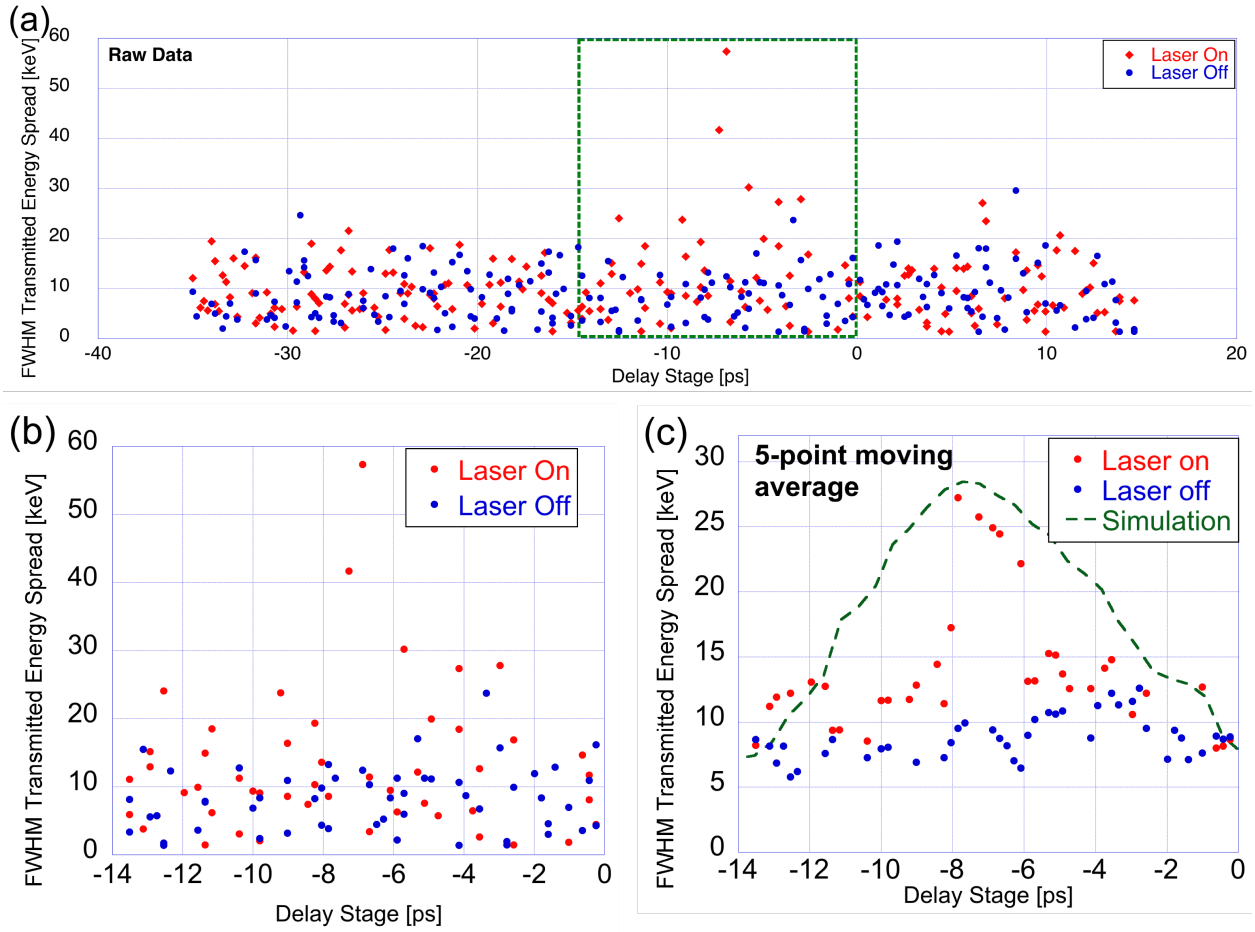

Figure 11: The width of the transmitted electron population versus the relative timing of the laser and electron beam, showing both laser-on (red) and laser-off (blue) shots. (a) Raw data over all delay stage positions and all widths. (b) Enlargement of previous graph, showing the relevant time window. The energy modulation during laser-on pulses is maximal near –7 ps delay. (c) The same data, smoothed using a 5-point moving average, and compared with simulation (assuming an ideal structure). Simulation results have been scaled.

Analysis & Implications

The experimental results presented here allow us to conclude with confidence that energy gain (acceleration) occurred in optimally aligned beams traversing the MAP resonant laser-powered structure. While the total energy gain and the gradient were modest, several factors were identified for the reduced performance compared to simulated and expected levels. Laser fluence increase, which would be well within current state-of-the-art, would have increased the acceleration gradient by a factor of 5 or more (limited by breakdown and material damage). In addition, fabrication challenges also contributed to the low accelerating gradient; though meeting these challenges is eminently possible within the current state-of-the-art in microfabrication, it would demand extensive process development (beyond what was possible under the work performed here). Nonetheless, these experimental results are significant: not only have we shown that relativistic particle beams can be accelerated in dielectric laser accelerator structures, but also that resonant standing-wave optical-scale structures can be operated in this challenging environment. In addition, the work evidences control of beam, alignment and tolerances at or near the level required for optical scale structures. While improvements clearly need to be made on all parameters, we have clearly demonstrated that the cumulative errors and variables involved can be controlled to the level required for signal measurement—an outcome that was not certain when the work commenced. It should be appreciated that a significant effort was required to detect and recover the signal from the "noise". Here the noise is actually a large background from electrons that are either not in phase or not in alignment with the accelerator. The ratio of correctly phased and aligned particles to incorrect particles is less than 1:100. By combining energy and time filtering along with numerical fits to various models, it was possible to extract the desired electron population and energy change signature. Such "filtering" is common in early advanced accelerator concepts experiments, and here represents a large mismatch from the beams generated in conventional accelerators to those which are ideal for DLA structures. Both the time structure, sub-femtosecond, and size scale, nanometer range, of ideal DLA beams are becoming of increasing interest for use in probing matter and interactions. Thus, there is already a strong effort to develop beams with desired properties, and future experiments on DLAs should strongly benefit from this concurrent work.

Laser powered accelerators and optical-scale structures have been considered in various forms for decades. Recent work, including that presented here, has brought to fruition a small number of functional structures capable of accelerating particle beams. With improved instruments and structure fabrication control these dielectric laser accelerators promise to bring relativistic and high-brightness beams to new applications and provide new capabilities to traditional applications. The laser has already become a ubiquitous laboratory tool; DLAs may provide the same technological shift to make particle accelerators universal laboratory instruments.

Executive Summary of Dissertation

A graduate student funded under this DTRA grant, Dr. Joshua Clarke McNeur, produced a doctoral dissertation in 2014 on the MAP structure and the experimental results. The dissertation is entitled, "The Micro-Accelerator Platform" and is available from the usual dissertation repositories. The summary below is from the dissertation's abstract:

Multiple applications in attosecond science, standoff nuclear detection, oil-well logging, and medicine require the use of compact high-gradient accelerators. The microstructure-based field of

Dielectric Laser Accelerators (DLA's) lever- ages high-power optical lasers and well-established nanofabrication techniques to accelerate electrons with GV/m electromagnetic fields over mm-scale distances, thus filling providing compact high-gradient acceleration. The Micro-Accelerator Platform (MAP) is a micron-scale slab-symmetric resonant-cavity DLA that accelerates electrons with a potential acceleration gradient approaching 1 GeV/m. In principle, electrons are synchronously accelerated as they traverse the standing wave resonance in the MAP's vacuum cavity, excited by a side-coupled Ti:Sapphire laser and confined by Distributed Bragg Reflectors above and be- low the vacuum cavity. Extensive analysis, simulations, and a proof-of-principle experiment show that the MAP is a viable candidate for compact high-gradient acceleration.

A simplified model of the MAP is used to develop analytic expressions of the resonant fields and associated forces in the vacuum cavity of the MAP. These resonant fields are shown to be capable of accelerating electrons with GeV/m acceleration gradients with no transverse defocusing.

To examine the dependence of the quality and frequency of the MAP's resonance on it's geometry and component materials, simulations in the frequency- domain EM solver HFSS and the time-domain EM solver and PIC code VORPAL are utilized. After a set of design parameters and materials that are practical to fabricate has been detailed, the quality of the MAP's resonance, spectral characteristics of the MAP, error tolerances of the design, ability of the resonance to accelerate electrons, and transverse dynamics of electrons traversing the MAP are presented via simulation results.

Optical lithography and sputtering deposition techniques are used to fabricate the final design of the MAP. After characterization of the fabricated sample is described, the testing of the MAP at the Next Linear Collider Test Accelerator is discussed. A 60 MeV electron beam traverses the MAP as it is illuminated by a Ti:Sapphire laser. The energy spectra of the beam after having passed through the illuminated MAP is then compared to the energy spectra of the beam after having passed through the MAP without laser illumination in order to deduce whether acceleration has occurred. The strength of acceleration versus the relative timing of the laser and electron beam is examined. It is deduced that for a subset of the data collected, the MAP accelerated electrons with a 50.6 MeV/m accelerating gradient. The implications of this finding and potential ways to increase the accelerating gradient are discussed.

Appendices

Simulations Used

Several publically available simulation packages were used throughout the research and described in the report as well as in past publications. The significant packages include:
VORPAL
HFSS
GEANT4
G4Beamline
elegant

Some custom software was written for processing data packages, translating between one data set and another and fitting data. These software are of a "utility" nature and do not necessarily represent new capabilities to the field.

Simulation Data

The simulations indicated above produce very large data files (e.g. a typical VORPAL run is several GB, and total storage well in excess of 1TB). Much of this intermediate data was culled after processing. The input files for runs are available and descriptions of how the simulations were performed are well detailed in the publications and the dissertation of J. McNeur.

Experimental Data

Large data sets (aprx 1TB) consisting primarily of images from the spectrometer beam monitor were taken over several experiments. The processed data sets are available and the most significant results are summarized in the included plots.

Publications Resulting from this Grant

1. "Fabrication of Micro-Scale Metallic and Dielectric Accelerator Structures with Sub-Wavelength Features" – E.R. Arab, G. Travish, N. Vartanian, J. Xu (UCLA) R.B. Yoder (Manhattanville College). FR5RFP013 Particle Accelerator Conference (May 4-8, 2009. Vancouver).

2. : "Testing of Laser-Driven Resonant Accelerating-Structures Possessing Sub-Wavelength Periodic Features" – N. Vartanian, G. Travish, J. Xu, E.R. Arab (UCLA) R.B. Yoder (Manhattanville College). FR5RFP014 Particle Accelerator Conference (May 4-8, 2009. Vancouver).

3. "Testing of a Laser-Powered, Slab-Symmetric Dielectric Structure for Medical and Industrial Applications" – S. Boucher (RadiaBeam) E.R. Arab, G. Travish, N. Vartanian (UCLA) R.B. Yoder (Manhattanville College). FR5RFP015 Particle Accelerator Conference (May 4-8, 2009. Vancouver).

4. E. R. Arab, *et al.,* "Initial Results on Electron Beam Generation Using Pyroelectric Crystals." International Particle Accelerator Conference (Kyoto, Japan, May 2010)

5. J. Zhou, *et al.*, "Fabrication of a Laser-Based Microstructure for Particle Acceleration." International Particle Accelerator Conference (Kyoto, Japan, May 2010)

6. J. McNeur, *et al.*, "A Tapered Dielectric Structure For Laser Acceleration At Low Energy." International Particle Accelerator Conference (Kyoto, Japan, May 2010)

7. R. B. Yoder, *et al.*, "Development of a Laser-Powered Dielectric Structure-Based Accelerator as a Stand-Alone Particle Source". Advanced Accelerator Concepts Workshop (Annapolis, MD, June 2010)

8. J. McNeur, *et al.*, "An Examination of Resonance, Acceleration, and Particle Dynamics in the Micro-Accelerator Platform". Advanced Accelerator Concepts Workshop (Annapolis, MD, June 2010)

9. J. Zhou, *et al.*, "Fabrication of a Prototype All-Dielectric Micro-Accelerator". Advanced Accelerator Concepts Workshop (Annapolis, MD, June 2010)

10. G. Travish, J. McNeur, J. Zhou, G. Liu, E. Sozer, K. S. Hazra, H. Yin, R. B. Yoder, "Experimental Progress Towards a Resonant Slab-Symmetric Dielectric Laser Accelerator," *Proceedings of IPAC2012,* paper WEPPP009, May 2012. Available at http://accelconf.web.cern.ch/AccelConf/IPAC2012/papers/weppp009.pdf

11. J. McNeur, G. Travish, H. Yin, R. B. Yoder, "Using Simulations To Understand Particle Dynamics and Resonance in the Micro-Accelerator Platform," *Proceedings of IPAC2012*, paper WEPPP006, May 2012. Available at http://accelconf.web.cern.ch/AccelConf/IPAC2012/papers/weppp006.pdf

12. G. Travish and R. B. Yoder, "Laser-powered dielectric-structures for the production of high-brightness electron and x-ray beams," *Laser Acceleration of Electrons*: *Proceedings of the SPIE* vol. 8079, paper 80790K, May 2011.

13. J. Zhou, J. McNeur, E. Arab, G. Travish, R. Yoder, "Fabrication of the micro accelerator platform for x-ray applications," *Advances in X-Ray/EUV Optics and Components: Proceedings of the SPIE* vol. 8139, paper 813928, August 2011.

14. G. Travish, "Dielectric Laser Accelerators: Are they viable advanced accelerator concepts?", *Proceedings of the Advanced Accelerator Concepts Workshop*, June 2012 (in press, AIP Conf. Proc.)

15. J. McNeur, K. S. Hazra, G. Liu, E. B. Sozer, G. Travish, R. B. Yoder, "Resonance, Particle Dynamics, and Particle Transmission in the Micro-Accelerator Platform," *Proceedings of the Advanced Accelerator Concepts Workshop*, June 2012 (in press, AIP Conf. Proc.).

16. J. McNeur, N. Carranza, E. B. Sozer, G. Travish, R. B. Yoder, "A Monolithic Relativistic Electron Beam Source Based on a Dielectric Laser Accelerator Structure," *Proceedings of the Advanced Accelerator Concepts Workshop*, June 2012 (in press, AIP Conf. Proc.).

17. J. McNeur, G. Travish, E. B. Sozer, K. S. Hazra, B. Matthews, R. J. England, K. Soong, E. Peralta, Z. Wu, and B. Montazeri, "Experimental Search For Acceleration In The Micro-Accelerator Platform," in *Proceedings of the 2013 International Particle Accelerator Conference* , May 2013, pp. 1307–1309. Available at http://accelconf.web.cern.ch/accelconf/IPAC2013/papers/tupea079.pdf

18. E. B. Sozer, J. McNeur, K. Hazra, G. Travish, E. Peralta, K. Soong, J. England, and R. Yoder, "Numerical Modeling And Experimental Data Analysis For Dielectric Laser Accelerators," in *Proceedings of the 2013 International Particle Accelerator Conference* , May 2013, pp. 1310–1312. Available at http://accelconf.web.cern.ch/accelconf/IPAC2013/papers/tupea080.pdf

19. R. B. Yoder and G. Travish, "Particle acceleration on a chip: A laser-driven micro-accelerator for research and industry," *Bulletin of the American Physical Society* **58**, 2013. Abstract available at http://absimage.aps.org/image/MAR13/MWS_MAR13-2012-003742.pdf

20. E. B. Sozer, J. McNeur, K. Hazra, G. Travish, and R. Yoder, "Experimental Progress Towards Laser Acceleration Of Relativistic Electrons With The Micro Accelerator Platform (MAP)" in *Proceedings of the 2013 IEEE Pulsed Power and Plasma Science Conference*, June 2013, in press.

21. J. McNeur, N. Carranza, G. Travish, Y. Hairong, and R. Yoder, "A monolithic relativistic electron beam source based on a dielectric laser accelerator structure," *AIP Conference Proceedings*, 1507, 464, 2012 (was in press during last report).

22. G. Travish, "Dielectric laser accelerators: Are they viable advanced accelerator concepts?," *AIP Conference Proceedings*, 1507, 85, 2012 (was in press during last report).

23. G. Travish, J. McNeur, J.Zhou, G. Liu, E. Sozer, KS Hazra, H. Yin, RB Yoder, "Experimental Progress Towards a Resonant Slab-Symmetric Dielectric Laser Accelerator," *AIP Conference Proceedings*, 1507, 85, 2012 (was in press during last report).

24. J. C. McNeur, "The Micro-Accelerator Platform," UCLA, 2014 (Ph.D. Dissertation).

25. [E. A. Peralta, K. Soong, R. J. England, E. R. Colby, Z. Wu, B. Montazeri, C. McGuinness, J. McNeur, K. J. Leedle, D. Walz, E. B. Sozer, B. Cowan, B. Schwartz, R. Byer, and G. Travish, "Demonstration of electron acceleration in a laser-driven dielectric microstructure," *Nature*, vol. 503, pp. 91–94, 2013.

26. B. Carlsten, F. Albert, S. Bajlekov, C. Barnes, K. Chouffani, E. Colby, E. Esarey, M. Fuchs, W. Graves, F. Hartemann, W. Leemans, R. Li, V. Litveneko, J. McVea, J. Mulroe, J. Osterhoff, D. Ratner, T. Raubenheimer, J. Rosenzweig, R. Ruth, W. Schlotter, M. Shverdin, G. Travish, F. Wang, V. Yakimenko, N. Yampolsky, and Y. Yan, "Novel Source Concepts Working Group Report," *portal.slac.stanford.edu*, 2010. [Online]. Available: https://portal.slac.stanford.edu/sites/ad_public/events/FLS2010/Documents/wg8.pdf. [Accessed: 21-Aug-2013].

27. J. Allen, G. Travish, H. Gong, and R. B. Yoder, "PROGRESS ON A LASER-DRIVEN DIELECTRIC STRUCTURE FOR USE AS A SHORT-PERIOD UNDULATOR," *Proceedings of FEL2012*. Review Articles.

28. J. C. McNeur, J. B. Rosenzweig, G. Travish, J. Zhou, R. B. Yoder, S. H. Gold, and G. S. Nusinovich, "An Examination of Resonance, Acceleration, and Particle Dynamics in the Micro-Accelerator Platform," presented at the ADVANCED ACCELERATOR CONCEPTS: 14th Advanced Accelerator Concepts Workshop, 2010, pp. 427–432.

29. P. Bermel, R. L. Byer, E. R. Colby, B. M. Cowan, J. Dawson, R. J. England, R. J. Noble, M. Qi, and R. B. Yoder, Nuclear Inst. and Methods in Physics Research, A **734**, 51 (2014).

30. R. J. England, R. J. Noble, K. Bane, D. H. Dowell, C.-K. Ng, J. E. Spencer, S. Tantawi, Z. Wu, R. L. Byer, E. Peralta, K. Soong, C.-M. Chang, B. Montazeri, S. J. Wolf, B. Cowan, J. Dawson, W. Gai, P. Hommelhoff, Y.-C. Huang, C. Jing, C. McGuinness, R. B. Palmer, B. Naranjo, J. B. Rosenzweig, G. Travish, A. Mizrahi, L. Schachter, C. Sears, G. R. Werner, and R. B. Yoder, "Dielectric laser accelerators," Reviews of Modern Physics, vol. 86, no. 4, pp. 1337–1389, Dec. 2014.

A news article was published on the progress in Dielectric Laser Accelerators and featuring our work on the MAP. This article was the result of Prof. Yoder's APS presentation and significant interactions between the PI and journalist.

The article is available in the June issue of the APS News:

http://www.aps.org/publications/apsnews/201306/chipscaleaccel.cfm

Publications Used in Preparing this report

1. S. V. Milton *et al.*, *Science* **292**, 2037 (2001).
2. J. Kern *et al*., *Science* **340**, 491 (2013).
3. S. Chatrchyan *et al.* (CMS collaboration), *Phys. Lett. B* **716**, 30 (2012).
4. V. Malka *et al.*, *Science* **298,** 1596 (2002).
5. I. Blumenfeld, *et al.*, *Nature* **445,** 7129 (2007).
6. B. M. Hegelich *et al*., *Nature* **439**, 441 (2006).
7. R. J. England *et al*., *Rev. Mod. Phys.* **86**, 1337 (2014).
8. C. K. Ng *et al*., *Phys. Rev. ST-AB* **13**, 121301 (2010).
9. B. Cowan, *Phys. Rev. ST-AB* **11**, 011301 (2008).
10. Z. Wu *et al*., *Phys. Rev. ST-AB* **17**, 081301 (2014).
11. E. A. Peralta *et al*., *Nature* **503**, 91-94 (2013).
12. J. Breuer, P. Hommelhoff, *Phys. Rev. Lett.* **111**, 134803 (2013).
13. R. B. Yoder, J. B. Rosenzweig, *Phys. Rev. ST-AB* **8**, 111301 (2005).
14. J. McNeur *et al*., AIP Conf. Proc. **1299**, 427 (2010).
15. J. McNeur *et al*., AIP Conf. Proc. **1507**, 470 (2012).
16. Ansys, Inc. (www.ansys.com).
17. Tech-X, Inc. (www.txcorp.com).
18. G. Travish *et al*., *Proc. 2012 Intl. Particle Accelerator Conf.,* paper WEPPP009, 2738–2740 (2012).
19. E. B. Sozer *et al.*, *Proc. 2013 Intl. Particle Accelerator Conf.,* paper TUPEA080 , 1310–1312 (2013).
20. M. Borland, Argonne National Laboratory Advanced Photon Source Technical Report No. LS-287, 2000.
21. T. J. Roberts, D. M. Kaplan, *Proc. 22nd Particle Accelerator Conf*., paper C070625, 3468–3470 (2007).

Department Of Defense

Defense Technical Information Center
8725 John J. Kingman Road, Suite 0944
Ft. Belvoir, VA 22060-6201
ATTN: DTIC/OCA

Defense Threat Reduction Information Analysis
Center 8725 John J. Kingman Road, Suite 0944
Ft. Belvoir, VA 22060-6201
ATTN: DTRIAC

Defense Threat Reduction Agency
8725 John J. Kingman Road
Ft. Belvoir, VA 22060-6201
ATTN: Dave Petersen